1-1-2012

Unidirectionally optical coupling from free space into silicon waveguide with wide flat-top angular efficiency

K Li

G Li

Feng Xiao
Edith Cowan University

Fan Lu

Zhonghua Wang

See next page for additional authors

10.1364/OE.20.018545
This is an Author's Accepted Manuscript of: Li, K., Li, G., Xiao, F. , Lu, F., Wang, Z., & Xu, A. (2012). Unidirectionally optical coupling from free space into silicon waveguide with wide flat-top angular efficiency. Optics Express, 20(17), 18545-18554. Available here

Unidirectionally optical coupling from free space into silicon waveguide with wide flat-top angular efficiency

Kun Li,[1] Guangyuan Li,[1,*] Feng Xiao,[2] Fan Lu,[1] Zhonghua Wang,[1] and Anshi Xu[1]

[1]*State Key Laboratory of Advanced Optical Communication Systems and Networks, School of Electronics Engineering and Computer Science, Peking University, Beijing, 100871, China*
[2]*WA Center of Excellence for MicroPhotonic System, Electron Science Research Institute, Edith Cowan University, Joondalup, WA, 6027, Australia*

*gyli_2008@hotmail.com

Abstract: A grating coupling scheme from free-space light into silicon waveguide with a remarkable property of wide flat-top angular efficiency is proposed and theoretically investigated. The coupling structure is composed of two cascaded gratings with a proper distance between their peak angular efficiencies. A quantitative semi-analytical theory based on coupled-mode models is developed for performance prediction and validated with the fully vectorial aperiodic Fourier modal method (a-FMM). With the theory, wide flat-top angular response is achieved and the conditions are pointed out. Proof-of-principle demonstrations show that the -1 dB angular width, a figure of merit to evaluate the flat-top performance, is broadened to almost 3 to 4 times, and meanwhile the -3 dB angular width, i.e., angular-full-width-half-maximum (AFWHM), is widened to nearly more than twice, compared with the reference gratings composed of the same number of periodic defects. We believe this work will find applications in biological or chemical sensing and novel optical devices.

OCIS codes: (050.1950) Diffraction gratings; (130.3120) Integrated optics devices.

References and links

1. T. W. Ang, G. T. Reed, A. Vonsovici, A. G. R. Evans, P. R. Routley, and M. R. Josey, "Effects of grating heights on highly efficient unibond SOI waveguide grating couplers," IEEE Photon. Technol. Lett. **12,** 59–61 (2000).
2. G. Roelkens, D. Vermeulen, D. V. Thourhout, R. Baets, S. Brision, P. Lyan, P. Gautier, and J. M. Fédéli, "High efficiency diffractive grating couplers for interfacing a single mode optical fiber with a nanophotonic silicon-on-insulator waveguide circuit," Appl. Phys. Lett. **92,** 131101 (2008).
3. M. A. Basha, S. Chaudhuri, and S. Safavi-Naeini, "A study of coupling interactions in finite arbitrarily-shaped grooves in electromagnetic scattering problem," Opt. Express **18,** 2743–2752 (2010).
4. D. Vermeulen, S. Selvaraja, P. Verheyen, G. Lepage, W. Bogaerts, P. Absil, D. V. Thourhout, and G. Roelkens, "High-efficiency fiber-to-chip grating couplers realized using an advanced CMOS-compatible silicon-on-insulator platform," Opt. Express **18,** 18278–18283 (2010).
5. S. Scheerlinck, J. Schrauwen, F. V. Laere, D. Taillaert, D. V. Thourhout, and R. Baets, "Efficient, broadband and compact metal grating couplers for silicon-on-insulator waveguides," Opt. Express **15,** 9625–9630 (2007).
6. G. Roelkens, D. V. Thourhout, and R. Baets, "High efficiency grating coupler between silicon-on-insulator waveguides and perfectly vertical optical fibers," Opt. Lett. **32,** 1495–1497 (2007).
7. D. Taillaert, W. Bogaerts, P. Bienstman, T. F. Krauss, P. V. Daele, I. Moerman, S. Verstuyft, K. D. Mesel, and R. Baets, "An out-of-plane grating coupler for efficient butt-coupling between compact planar waveguides and single-mode fibers," IEEE J. Quantum Electron. **38,** 949–955 (2002).

#166982 - $15.00 USD Received 18 Apr 2012; revised 20 Jul 2012; accepted 22 Jul 2012; published 30 Jul 2012

8. F. V. Laere, G. Roelkens, M. Ayre, J. Schrauwen, D. Taillaert, D. V. Thourhout, M. F. Krauss, and R. Baets, "Compact and highly efficient grating couplers between optical fiber and nanophotonic waveguides," J. Lightwave Technol. **25,** 151–156 (2007).
9. L. Vivien, D. Pascal, S. Lardenois, D. Marris-Morini, E. Cassan, F. Grillot, S. Laval, J. M. Fédéli, and L. E. Melhaoui, "Light injection in SOI microwaveguides using high-efficiency grating couplers," J. Lightwave Technol. **24,** 3810–3815 (2006).
10. G. Maire, L. Vivien, G. Sattler, A. Kazmierczak, B. Sanchez, K. B. Gylfason, A. Griol, D. Marris-Morini, E. Cassan, D. Giannone, H. Sohlström, and D. Hill, "High efficiency silicon nitride surface grating couplers," Opt. Express **16,** 328–333 (2008).
11. J. Wu, G. Zheng, Z. Li, and C. Yang, "Focal plane tuning in wide-field-of-view microscope with Talbot pattern illumination," Opt. Lett. **36,** 2179–2181 (2011).
12. J. Ho, A. V. Parwani, D. M. Jukic, Y. Yagi, L. Anthony, and J. R. Gilbertson, "Use of whole slide imaging in surgical pathology quality assurance: design and pilot validation studies," Hum. Pathol. **37,** 322–331 (2006).
13. S. Nagrath, L. V. Sequist, S. Maheswaran, D. W. Bell, D. Irimia, L. Ulkus, M. R. Smith, E. L. Kwak, S. Digumarthy, A. Muzikansky, P. Ryan, U. J. Balis, R. G. Tompkins, D. A. Haber, and M. Toner, "Isolation of rare circulating tumour cells in cancer patients by microchip technology," Nature **450,** 1235–1239 (2007).
14. A. F. Coskun, I. Sencan, T. W. Su, and A. Ozcan, "Lensless wide-field fluorescent imaging on a chip using compressive decoding of sparse objects," Opt. Express **18,** 10510–10523 (2010).
15. K. L. Lee, C. W. Lee, W. S. Wang, and P. K. Wei, "Sensitive biosensor array using surface plasmon resonance on metallic nanoslits," J. Biomed. Opt. **12,** 044023 (2007).
16. E. D. Tommasi, L. D. Stefano, I. Rea, V. D. Sarno, L. Rotiroti, P. Arcari, A. Lamberti, C. Sanges, and I. Rendina, "Porous silicon based resonant mirrors for biochemical sensing," Sensors **8,** 6549–6556 (2008).
17. A. Sentenac and A. Fehrembach, "Angular tolerant resonant grating filters under oblique incidence," J. Opt. Soc. Am. A **22,** 475–480 (2005).
18. A. B. Greenwell, S. Boonruang, and M. G. Moharam, "Multiple wavelength resonant grating filters at oblique incidence with broad angular acceptance," Opt. Express **15,** 8626–8638 (2007).
19. M. Born and E. Wolf, *Principles of Optics* (Cambridge University Press, 1999).
20. H. Liu, P. Lalanne, X. Yang, and J. P. Hugonin, "Surface plasmon generation by subwavelength isolated objects," IEEE J. Sel. Top. Quantum Electron. **14,** 1522–1529 (2008).
21. D. Taillaert, F. V. Laere, M. Ayre, W. Bogaerts, D. V. Thourhout, P. Bienstman, and R. Baets, "Grating couplers for coupling between optical fibers and nanophotonic waveguides," Jpn. J. Appl. Phys. **45,** 6071–6077 (2006).
22. L. Dong, S. Iyer, S. Popov, and A. Friberg, "3D fabrication of waveguide and grating coupler in SU-8 by optimized gray scale electron beam lithography," in *Proceedings of ACP* (2010).
23. A. Sure, T. Dillon, J. Murakowski, C. Lin, D. Pustai, and D. W. Prather, "Fabrication and characterization of three-dimensional silicon tapers," Opt. Express **11,** 3555–3561 (2003).
24. S. Lardenois, D. Pascal, L. Vivien, E. Cassan, S. Laval, R. Orobtchouk, M. Heitzmann, N. Bouzaida, and L. Mollard, " Low-loss submicrometer silicon-on-insulator rib waveguides and corner mirrors," Opt. Lett. **28,** 1150–1152 (2003).
25. G. Li, F. Xiao, L. Cai, K. Alameh, and A. Xu, "Theory of the scattering of light and surface plasmon polaritons by finite-size subwavelength metallic defects vis field decomposition," New J. Phys. **13,** 073045 (2011).
26. G. Li, L. Cai, F. Xiao, Y. Pei, and A. Xu, "A quantitative theory and the generalized Bragg condition for surface plasmon Bragg reflectors," Opt. Express **18,** 10487–10499 (2010).

1. Introduction

In photonic integrated circuits (PICs), an important issue in engineering-related optical devices is to efficiently couple freely-propagating light into waveguides and to control the direction in which they are incoupled. Grating-assisted couplers present a feasible and efficient approach, since they represent an enabling technology with high integration density and relatively low loss [1, 2]. With the advantage of high coupling efficiency, no need for a cleaved facet, and opening a way for wafer-scale testing, various grating couplers have been theoretically analyzed and experimentally demonstrated during the last decade [3–8]. Currently, most works were focused on improving the coupling efficiency for a specific designed angle such as $\theta = 0^\circ$ [7] or $\theta = 10^\circ$ [8]. They suffer from a very tight angular tolerance with angular-full-width-half-maximum (AFWHM) usually being 3° [9] or 4° [10]. In other words, the coupling efficiency decreases rapidly if θ deviates from the designed angle. As a result, strict alignment is a necessary requirement. Yet in some applications such as imaging or detecting mixed green algae slide [11], whole-slide digital pathology diagnosis [12], rare-cell detection and analysis in large

#166982 - $15.00 USD Received 18 Apr 2012; revised 20 Jul 2012; accepted 22 Jul 2012; published 30 Jul 2012

area micro-fluidic devices [13], and wide-field fluorescent imaging [14], the ability to collect wide-angle targets is highly desirable. Specially, in biological or chemical sensing [15, 16], the light scattered by the analytes may normally or obliquely impinge upon detectors, and incidence is generally unpredictable. In this case, it is favorable for the waveguide or fiber which is used to collect scattered light into detectors or spectrometers to have a broad angular response, alleviating the alignment and resulting in real-time sensing. In other words, alleviating angular tolerance and realizing wide flat-top angular response is a crucial issue. To the best of our knowledge, however, little work has hitherto addressed the issue of broadening the angular efficiency for coupling free-space light into waveguide, except the work to increase the angular tolerance of grating filter making use of bi-atom grating [17] and multilayer waveguides [18].

Before we address this challenge, let us retrospect the angular resolution of a diffraction limited system, i.e. the Rayleigh criterion [19], as illustrated in Fig. 1. When two objects are separated by a small angle, the diffraction patterns overlap as shown in Fig. 1(a). It is able to resolve the two objects as long as the central peaks in the two diffraction patterns don't overlap as illustrated in Fig. 1(c). The minimum resolvable detail is when one central peak falls below the first minimum of the other diffraction pattern as shown in Fig. 1(b). If the plots are for angular coupling efficiency, it is clear that the case of Fig. 1(b) with a proper separation between angular peaks will lead to wide flat-top response and wide AFWHM.

As a proof of concept, in this paper we propose a unidirectional coupling scheme of wide flat-top angular efficiency by cascading two gratings that are of proper distance between their peak angular efficiencies, as illustrated in Fig. 2(a). A quantitative theory based on coupled-mode models will be developed for the performance prediction of the proposed structure. Based on the semi-analytical theory, the conditions for realizing wide flat-top angular response are pointed out. The theory will also be validated by comparing with computational results using the fully vectorial aperiodic Fourier modal method (a-FMM) [20]. The performance, the conditions, and the cost will be analyzed and discussed. Finally, the conclusions will be summarized.

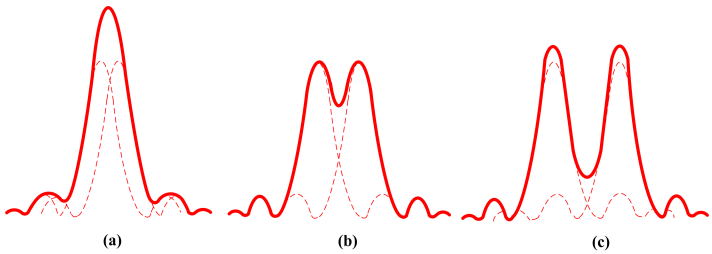

Fig. 1. The overlapping diffraction patterns: (a) light waves from two objects are unresolved; (b) Rayleigh criterion; (c) light waves from two objects are resolved.

2. Quantitative semi-analytical theory

Figure 2(a) illustrates the schematic of proposed unidirectional coupling structure. The grating coupling structure is based on a silicon-on-insulator (SOI) wafer, consisting of a 240 nm silicon waveguide layer and a 900 nm buried oxide layer on a silicon substrate. First, following the deposition of a blanket SiO_2 hard mask, the silicon overlay is locally defined by epitaxial silicon growth [2] to obtain 250nm silicon overlay thickness in the grating region. The taper and the photonic wire are then defined using e-beam lithography [21] and etched 240 nm deep by inductively coupled plasma (ICP). After that, one may use the gray-scale electron-beam lithography [22] followed by ICP etching [23] to produce triangular pattern of the grating. In practice, the triangular pattern are approximated by 20-step staircases. As the design and fabrication of

#166982 - $15.00 USD Received 18 Apr 2012; revised 20 Jul 2012; accepted 22 Jul 2012; published 30 Jul 2012

the taper and photonic wire has a well-rounded study [8, 9, 24], here we focus on the design of the grating, which can be fabricated using state-of-the-art techniques just as stated above, to achieve wide flat-top angular efficiency.

Considering that the single-mode waveguides are commonly used for the coupling of light according to previous works [8, 9, 24], the parameters of the waveguide should be properly chosen firstly to make sure single-mode operation for TM polarization. Throughout this paper, the calculations are performed with λ = 1550 nm, t_s = 240 nm, t_c = 900 nm, n_s = 3.518 (Si), n_c = 1.46 (SiO_2). In this case, the optical waveguide only support the fundamental TM mode. Note that it is clear that there are so many parameters that pure simulations using finite difference time domain (FDTD) method or finite element method (FEM) suffer from high numerical cost and aimless parameters scan. To circumvent these problems, here we develop a quantitative theory based on coupled-mode model to provide parameters optimization with a clear picture of physics. We emphasize that although TM polarized plane wave is used as the example throughout the paper, the concept and the theory also work for TE polarization.

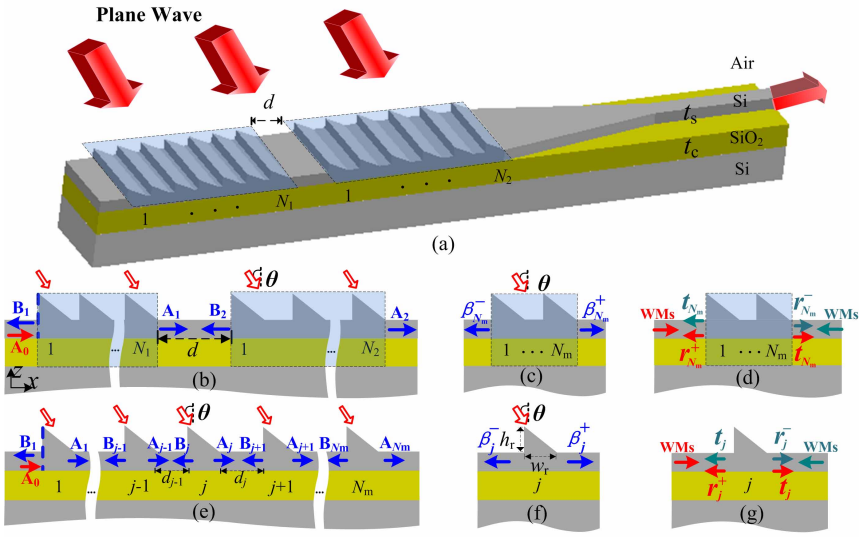

Fig. 2. (a) Schematic of the proposed grating coupler. (b) Schematic of the global model, which treats each array of grating as a 'black box'. The first (or the second) 'black box' is composed of N_1 (or N_2) periodic defects with period p_1 (or p_2). The defects in both 'black boxes' are of constant height h_r and width w_r. The structural distance between two 'black boxes' is d. (c,d) show the main elementary scattering processes for the 'black box' of N_m defects, i.e., the excitation coefficients $\beta^{\pm}_{N_m}$, reflection coefficients $r^{\pm}_{N_m}$ and transmission coefficient t_{N_m} under illumination of plane wave (c) and waveguide modes (d). (e) schematic of the nested model of an isolated 'black box'. (f,g) show the scattering coefficients of a single defect under illumination of plane wave (f) and waveguide mode (g). The vertical blue-dashed lines in (b,e) indicate the zero phase of the incident plane wave.

In the case of single-mode operation, a semi-analytical theory is developted in form of two nested models: a global model that treats the protuberance arrays as two 'black boxes' exciting, reflecting and transmitting waveguide modes (WMs), and focuses on the 'box-to-box' distance d, as illustrated in Figs. 2(b)-2(d); and a nested model on the excitation, reflectance and transmittance coefficients of WMs by the 'black boxes', as shown in Figs. 2(e)-2(g). The nested theoretical models bridge the scattering coefficients of the finite-size protuberances to those of a single one, resulting in a great reduction of the computational cost.

#166982 - $15.00 USD Received 18 Apr 2012; revised 20 Jul 2012; accepted 22 Jul 2012; published 30 Jul 2012

The global model is shown in Fig. 2(b), where B_1 (or B_2) and A_1 (or A_2) are the respective complex amplitudes of magnetic field H_y of the backward- and forward-going WMs away from the first (or the second) 'black box'. The main elementary scattering processes involved in the proposed model are shown in Figs. 2(c) and 2(d): $\beta^+_{N_m}$ and $\beta^-_{N_m}$ are the excitation coefficients of forward- and backward-going WMs by the 'black box' with N_m defects under the plane wave illumination, respectively; $r^+_{N_m}$ and $r^-_{N_m}$ are the reflectance coefficients of forward- and backward-going WMs, respectively; t_{N_m} is the transmittance coefficient. The coupled-mode equations lead to:

$$B_1 = \beta^-_{N_1} + t_{N_1} u B_2 + r^+_{N_1} u A_0 \tag{1a}$$

$$A_1 = \beta^+_{N_1} + r^-_{N_1} u B_2 + t_{N_1} u A_0 \tag{1b}$$

$$B_2 = w\beta^-_{N_2} + r^+_{N_2} u A_1 \tag{1c}$$

$$A_2 = w\beta^+_{N_2} + t_{N_2} u A_1 \tag{1d}$$

where $w = \exp[ik_0(p_1 N_1 - p_1 + w_r + d)\sin\theta]$ is the phase shift introduced by the incident plane wave. This is because the zero phase is assumed to be at the leftmost side of the first 'black box' for the calculation of $\beta^\pm_{N_1}$ ($x = z = 0$); whereas it is at the leftmost side of the second 'black box' for the calculation of $\beta^\pm_{N_2}$ ($x = p_1 N_1 - p_1 + w_r + d, z = 0$). d is the structural distance between the two 'black boxes'. $u = \exp(ik_0 n_{\text{eff}} d)$ with n_{eff} being the complex effective refractive index of the waveguide mode. Note that $t_{N_m} = t^+_{N_m} = t^-_{N_m}$ according to the principle of optical reversibility. We emphasize the propagation losses of the WMs have been embodied via complex n_{eff}. To calculate the WMs excitation coefficients, $\beta^+_{N_1N_2} = A_2$, $\beta^-_{N_1N_2} = B_1$, one sets $A_0 = 0$; whereas to calculate the WMs reflectance and transmittance coefficients, $r_{N_1N_2} = B_1/(uA_0)$ and $t_{N_1N_2} = A_2/uA_0$, one sets $\beta^\pm_{N_1} = 0$ and $\beta^\pm_{N_2} = 0$. Then the WMs excitation, reflection and transmission coefficients of the cascaded 'black boxes' are obtained after a series of algebraic operation:

$$\beta^+_{N_1N_2} = w\beta^+_{N_2} + t_{N_2} u \frac{r^-_{N_1} uw\beta^-_{N_2} + \beta^+_{N_1}}{1 - r^-_{N_1} r^+_{N_2} u^2}, \tag{2a}$$

$$\beta^-_{N_1N_2} = \beta^-_{N_1} + t_{N_1} u \frac{w\beta^-_{N_2} + r^+_{N_2} u\beta^+_{N_1}}{1 - r^-_{N_1} r^+_{N_2} u^2}, \tag{2b}$$

$$r_{N_1N_2} = r^+_{N_1} + r^+_{N_2} \frac{t^2_{N_1} u^2}{1 - r^-_{N_1} r^+_{N_2} u^2}, \tag{2c}$$

$$t_{N_1N_2} = \frac{t_{N_1} t_{N_2} u}{1 - r^-_{N_1} r^+_{N_2} u^2}, \tag{2d}$$

where $\beta^+_{N_1N_2}$ is dominated by $w\beta^+_{N_2}$ in Eq. (2a) as $|t_{N_2}|$ is usually small when $|\beta^+_{N_2}|$ is optimized. Similarly, $\beta^-_{N_1}$ dominates in $\beta^-_{N_1N_2}$ in Eq. (2b).

Because the second 'black box' is designed to unidirectionally couple free-space light into the desired waveguide direction and suppress coupling in the opposite direction (i.e., $|\beta^-_{N_2}| \ll |\beta^+_{N_2}|$), it is reasonable to ignore the term $w\beta^-_{N_2} u r^-_{N_1} u t_{N_2}$. Moreover, the multiple reflections between the two 'black boxes' $r^-_{N_1} r^+_{N_2} u^2$ are negligible because $|r^-_{N_1} r^+_{N_2} u^2| \ll 1$. Then Eq. (2a) is simplified into

$$\beta^+_{N_1N_2} \approx t_{N_2} u\beta^+_{N_1} + w\beta^+_{N_2} \tag{3}$$

The physical interpretations of Eq. (3) is intuitively meaningful as illustrated in Fig. 3. It means the interference between the forward-going WMs by the transmission of the excitation

#166982 - $15.00 USD Received 18 Apr 2012; revised 20 Jul 2012; accepted 22 Jul 2012; published 30 Jul 2012

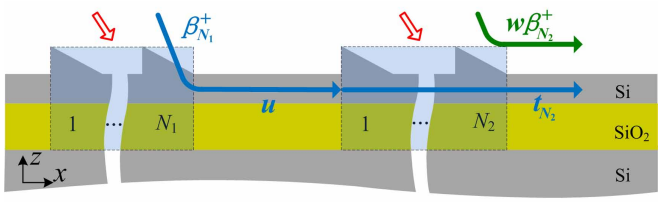

Fig. 3. Physical interpretations of Eq. (3).

of the first 'black box' $t_{N_2}u\beta_{N_1}^+$ (blue arrow) and by the excitation of the second 'black box' $w\beta_{N_2}^+$ (green arrow). This recalls the above-mentioned concept to realize wide flat-top angular response as shown in Fig. 1(b). In Eq. (3), t_{N_2} and u play key roles of phase modulation of $\beta_{N_1}^+$. If $\beta_{N_1}^+$ and $\beta_{N_2}^+$ are first designed properly with comparable incoupling coefficients and suitable angular interval between peak incoupling coefficients, it is possible to obtain wide flat-top angular response for $\beta_{N_1N_2}^+$ provided the structural distance between the two 'black boxes' is given by

$$\arg(t_{N_2}) + k_0 \mathrm{Re}(n_{\mathrm{eff}})d \approx 2m\pi \tag{4}$$

where the functions 'arg' and 'Re' refer to the argument and the real part, respectively, and m is an integer.

Now let us consider the excitation, reflectance and transmittance coefficients of WMs by the 'black box', which may be consist of N aperiodic defects with arbitrary distances $d_j (j = 1, ..., N-1)$ as shown in Fig. 2(e). Following our pervious work [25, 26], the corresponding coefficients of an isolated 'black box' of N defects are given by:

$$\beta_N^+ = \frac{w_{N-1}(\beta_1^+ + t_1 r_{N-1}^- u_{N-1}^2 \beta_1^-)}{1 - t_1 u_{N-1} w_{N-1}^{-1}}, \tag{5a}$$

$$r_N = r_{N-1}^+ + r_1^+ \frac{t_{N-1}^2 u_{N-1}^2}{1 - r_1^+ r_{N-1}^- u_{N-1}^2}, \tag{5b}$$

$$t_N = \frac{t_1 t_{N-1} u_{N-1}}{1 - r_1^+ r_{N-1}^- u_{N-1}^2}. \tag{5c}$$

Where $u_{N-1} = \exp(ik_0 n_{\mathrm{eff}} d_{N-1})$, $w_{N-1} = \exp[ik_0(Nw_r - w_r + \sum_1^{N-1} d_j)\sin\theta]$. In some cases, the equations will be reduced into simplified forms. For example, for periodic symmetric defects, $u_j = u$, $w_j = w^j$, and $r_j = r_j^- = r_j^+$ for $j = 1, \cdots, N-1$, $|r_1^+ r_{N-1}^- u_{N-1}^2| \ll 1$, Eq. (5) is then reduced into

$$\beta_N^+ = \frac{w^{N-1}(\beta_1^+ + t_1 r_{N-1} u^2 \beta_1^-)}{1 - t_1 u w^{1-N}}, \tag{6a}$$

$$r_N = r_{N-1} + r_1 t_{N-1}^2 u^2, \tag{6b}$$

$$t_N = t_1 t_{N-1} u. \tag{6c}$$

We emphasize that the nested model is versatile for a general grating composed of periodic or aperiodic defects, where the defect may be of various geometries and refractive index profiles, as their influences have been embodied via $\beta_1^\pm$, $r_1^\pm$ and t_1.

For simplicity, hereafter we restrict ourselves to periodic defects, i.e., $d_1 = ... = d_{N-1} = p - w_r$. β_N^+, r_N and t_N can be calculated recursively starting from $\beta_1^\pm$, $r_1^\pm$ and t_1, thus the geometry optimization for N periodic defects is reduced into that for a single one. The constructive

#166982 - $15.00 USD Received 18 Apr 2012; revised 20 Jul 2012; accepted 22 Jul 2012; published 30 Jul 2012

interference condition of β_N^+ is obtained from Eq. (5a):

$$\arg(t_1) + k_0 \mathrm{Re}(n_{\mathrm{eff}})p - k_0 n_0 p \sin\theta = 2m\pi \tag{7}$$

We refer to Eq. (7) as the generalized grating equation. Compared with the conventional grating equation, the generalized one is versatile for a general grating composed of various defects. Specially, for gratings composed of high-index dielectric protuberances, the additional term $\arg(t_1)$ is quite important since it may be relatively large in this case.

3. Results and discussions

In this section, the grating coupling scheme to achieve wide flat-top response by properly cascading two gratings is validated with proof-of-principle demonstrations. The semi-analytical theory is quantitatively validated using exhaustive calculations with various grating parameters by comparing with simulations using the a-FMM. With the theory, wide flat-top angular efficiency is achieved and the conditions and versatility for various shaped defects are pointed out.

The incident plane wave is normalized such that its Poynting vector is unitary [20]. Under this normalized condition, the incoupling cross section $|\beta_N^+|^2$ means the power flow carried by the forward-going WMs, and the coupling efficiency $\eta_N^+ = |\beta_N^+|^2/D$ with D being the grating cross section represents the ratio of the forward-going WMs power flux to the incident power flux that launches into the gratings. To evaluate the performance of wide flat-top angular coupling efficiency, we adopt -1 dB angular width Φ and -3 dB angular width Θ as the figures of merit (FoMs), which are defined as the angular range between two specified angle cut-off points that are -1 dB and -3 dB below the peak angular efficiency, respectively. Specifically, Φ is used to evaluate flat-top angular response while Θ is AFWHM.

Figure 4 compares coupling efficiency $\eta_{N_1+N_2}^+$ of the reference grating with N_1+N_2 defects of period p_1 (blue-solid line) or p_2 (black-solid line) in (b,e,h,k) with the model predictions (green-dashed line with circles) and the a-FMM data (red-solid line) on the above-mentioned $\eta_{N_1N_2}^+$ of the cascaded gratings. As shown in Fig. 4, by properly cascading two isolated gratings (a,d,g,j), flat-top angular response of $\eta_{N_1N_2}^+$ is realized and the AFWHM is broadened in (c,f,i,l): Φ is broadened to almost 3 to 4 times and meanwhile Θ is widened to nearly more than twice compared with the reference ones (b,e,h,k). The angular coupling efficiency peaks up to values of 0.28, 0.36, 0.33, 0.31 average for (b,e,h,k) and 0.16, 0.18, 0.15, 0.14 for (c,f,i,l), respectively. More specifically, compared with the reference grating, Φ of the cascaded grating are broadened to almost 3 to 4 times at an acceptable cost of decreasing the peak coupling efficiency only by nearly half. It is also clearly shown that when the cascaded gratings are optimized for other different incidence angles ([d,e,f],[g,h,i]) or of a higher number of defects (j,k,l), the grating coupling scheme is still valid. Moreover, since the incoupling cross section $|\beta_{N_1N_2}^+|^2$ is dominated by $|\beta_{N_2}^+|^2$, as we have stated previously, the second angular peak position (black-dashed line) of $\eta_{N_1N_2}^+$ (c,f,i,l) remains almost consistent with that of $\eta_{N_2}^+$ (a,d,g,j) as expected, whereas for the first angular peak with regard to $\eta_{N_1}^+$, there is an offset introduced by t_{N_2}.

Figure 5 illustrates the importance of the conditions for wide-flat top angular efficiency, i.e., the two 'black boxes' should be of proper structural distance d (a,b), comparable incoupling cross sections (c,d) and suitable angular interval (e,f). There will be no wide flat-top angular coupling efficiency if d deviates from the model prediction given by Eq. (4) (a,b), peak values of incoupling cross sections are not comparable (c,d), or the angular interval between the peaks of $\eta_{N_1}^+$ and $\eta_{N_2}^+$ is too small (e,f) or too large (not shown).

Moreover, the accuracy of the theory has been quantitatively validated by comparing with a-FMM calculations, as shown in Figs. 4 and 5. We emphasize that the theory, which incorporates

#166982 - $15.00 USD Received 18 Apr 2012; revised 20 Jul 2012; accepted 22 Jul 2012; published 30 Jul 2012

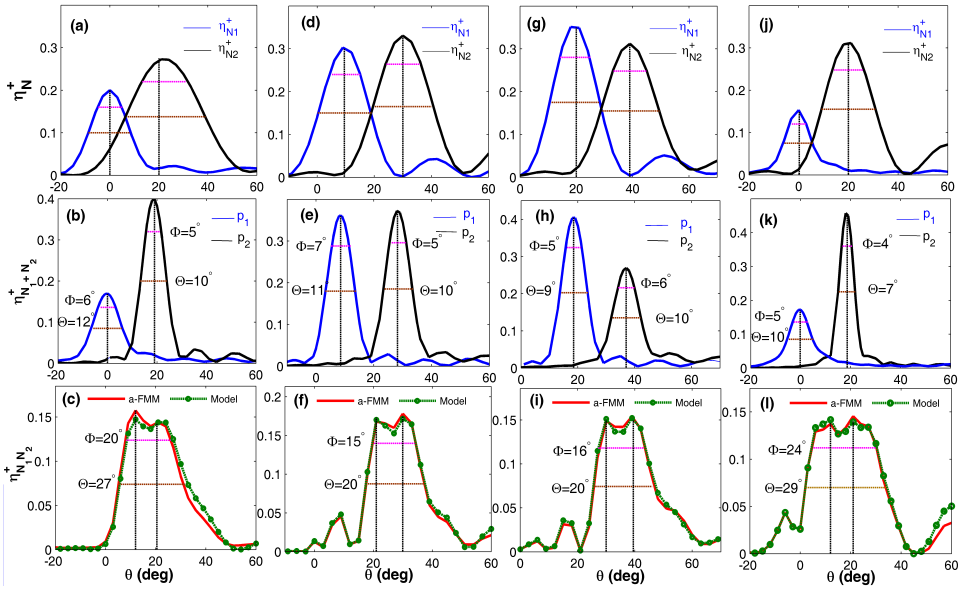

Fig. 4. Comparisons among coupling efficiency of the isolated grating $\eta_N^{\pm}$ with N_1 or N_2 defects (top row), the reference grating $\eta_{N_1+N_2}^{\pm}$ with N_1+N_2 defects of period p_1 (or p_2) (middle row), and the cascaded gratings $\eta_{N_1N_2}^{\pm}$ with N_1 defects of period p_1, N_2 defects of period p_2, and 'box-to-box' structural distance d (bottom row) by model predictions (green-dashed lines with circles) and a-FMM computational data (red-solid lines). The vertical black-dashed lines indicate the peak angular positions. The calculation of the four columns from left to right by a-FMM are performed for: $h_r = 250$ nm, $w_r = 520$ nm, (a,b,c) $p_1 = 567$ nm, $N_1 = 8$, $p_2 = 675$ nm, $N_2 = 4$, and $d = 240$ nm; (d,e,f) $p_1 = 617$ nm, $N_1 = 7$, $p_2 = 740$ nm, $N_2 = 6$, and $d = 1150$ nm; (g,h,i) $p_1 = 675$ nm, $N_1 = 7$, $p_2 = 811$ nm, $N_2 = 6$, and $d = 1195$ nm. (j,k,l) $p_1 = 567$ nm, $N_1 = 14$, $p_2 = 675$ nm, $N_2 = 6$, and $d = 720$ nm; Φ is broadened from 6° or 5° to 20° (b,c), from 7° or 5° to 15° (e,f), from 5° or 6° to 16° (h,i), and from 5° or 4° to 24° (k,l), respectively; Θ is widened from 12° or 10° to 27° (b,c), from 11° or 10° to 20° (e,f), from 9° or 10° to 20° (h,i), and from 10° or 7° to 29° (h,i), respectively.

interlinks among the key parameters with clear physical pictures, is very efficient and flexible. One only needs to scan $\beta_1^{\pm}$, $r_1^{\pm}$ and t_1 of a single defect instead of $\beta_N^{\pm}$, $r_N^{\pm}$ and t_N of N defects as functions of w_r and h_r. $\beta_N^{\pm}$, $r_N^{\pm}$ and t_N for various grating numbers or periods are then obtained with the nested models at negligible computational cost. This cost reduction is especially remarkable when one needs to increase N to improve the performance. More importantly, there are no restrictions on the defect's geometry and refractive index profile in the theoretical model. Apart from the above mentioned triangular shaped defect, the proposed method is also versatile for a deep etched (Fig. 6) or fully etched (not shown) rectangular grating. As clearly seen from Figs. 6(a)-6(d), the scattering coefficients of each 'black-box' composed of periodic rectangular grooves is able to be predicted with a high accuracy, in both amplitudes and phases. As a result, a flat-top angular efficiency is also achieved using the theoretical model: Φ is broadened to 3-4 times and meanwhile Θ is widened to more than 3 times compared with the reference one (e) as depicted in Figs. 6(e)-6(f). We should note that as the theoretical model is developed for single-mode waveguide, it is only suitable for the case of single-mode operation.

#166982 - $15.00 USD Received 18 Apr 2012; revised 20 Jul 2012; accepted 22 Jul 2012; published 30 Jul 2012

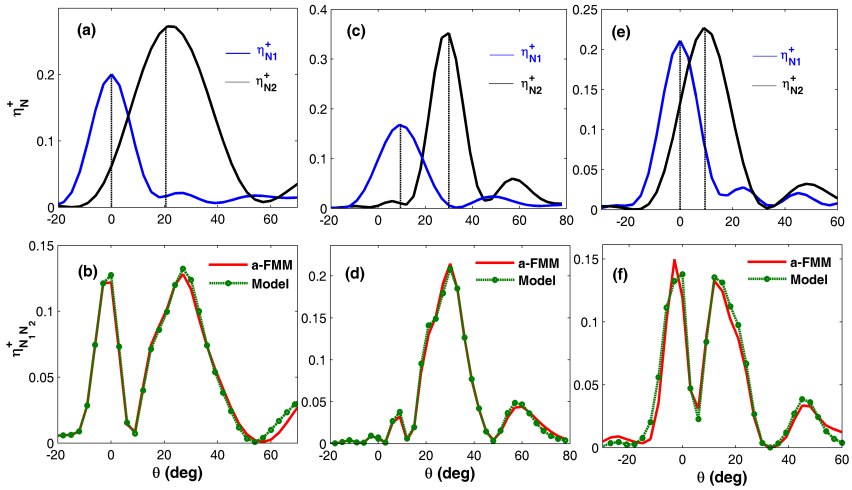

Fig. 5. Influential elements on wide-flat top angular efficiency: (a,b) structural distance, (c,d) peak incoupling cross sections, and (e,f) the interval between angular peaks. The vertical black-dashed lines indicate the peak angular positions. The calculation of the three columns from left to right by a-FMM are performed respectively for: $h_r = 250\,\text{nm}$, $w_r = 520\,\text{nm}$, (a,b) $p_1 = 567\,\text{nm}$, $p_2 = 675\,\text{nm}$, $N_1 = 8$, $N_2 = 4$, and $d = 490\,\text{nm}$; (c,d) $p_1 = 617\,\text{nm}$, $p_2 = 740\,\text{nm}$, $N_1 = 6$, $N_2 = 8$, and $d = 905\,\text{nm}$; (e,f) $p_1 = 567\,\text{nm}$, $p_2 = 617\,\text{nm}$, $N_1 = 9$, $N_2 = 6$, and $d = 495\,\text{nm}$, respectively.

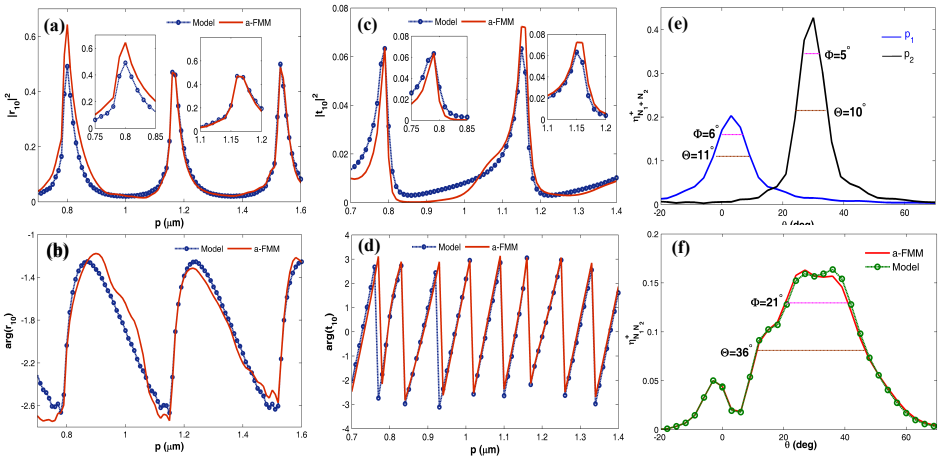

Fig. 6. The calculations are performed for deeply etched rectangular grating with groove depth $h_r = 100\,\text{nm}$ and width $w_r = 150\,\text{nm}$. (a-d) depict the comparison of the model predictions (blue-dashed line with circles) and the a-FMM computational data (red line) for 10 periodic grooves on (a) $|r_{10}|^2$, (b) $\arg(r_{10})$, (c) $|t_{10}|^2$, and (d) $\arg(t_{10})$ as functions of the period p. (e,f) show the comparison between the reference rectangular grating $\eta^+_{N_1+N_2}$ with N_1+N_2 defects of period p_1 or p_2 (e), and the cascaded rectangular grating $\eta^+_{N_1N_2}$ with N_1 defects of period p_1, N_2 defects of period p_2, and 'box-to-box' structural distance d (f). $p_1 = 809\,\text{nm}$, $p_2 = 1057\,\text{nm}$, $N_1 = 6$, $N_2 = 4$, and $d = 630\,\text{nm}$.

#166982 - $15.00 USD Received 18 Apr 2012; revised 20 Jul 2012; accepted 22 Jul 2012; published 30 Jul 2012

4. Conclusions

In conclusion, we have proposed and investigated a grating coupling scheme from free-space light into silicon waveguide with a remarkable property of wide flat-top angular efficiency. A semi-analytical theory in form of two nested coupled-mode models has been developed for performance prediction and parameters optimization. Comparisons of the model predictions with a-FMM calculations have shown that all the salient feature is quantitatively captured by the model. The theoretical model is versatile for a general grating composed of periodic or aperiodic defects, where the defect may be of various geometries and refractive index profiles. With the theory, the conditions for wide flat-top angular response have been pointed out, i.e., the cascaded gratings should be of proper structural distance, comparable peak incoupling cross sections and suitable angular interval. Proof-of-principle demonstrations have shown that: compared with the reference gratings composed of the same number of periodic defects, the -1 dB angular width Φ, a figure of merit to evaluate the flat-top performance, is broadened to almost 3 to 4 times; and meanwhile the -3 dB angular width Θ, i.e., angular-full-width-half-maximum (AFWHM), is widened to nearly more than twice, at an acceptable cost of decreasing angular coupling efficiency only by half. We believe that this work may be of great interest for use in novel optical devices and biological or chemical sensing.

Acknowledgments

This work was supported by the National Natural Science Foundation of China (NSFC) under grant 61107065, China Postdoctoral Science Foundation, and the State Key Laboratory of Advanced Optical Communication Systems and Networks, China.

#166982 - $15.00 USD Received 18 Apr 2012; revised 20 Jul 2012; accepted 22 Jul 2012; published 30 Jul 2012